Applied Surface Science 255 (2009) 7517–7523

Contents lists available at ScienceDirect

Applied Surface Science

journal homepage: www.elsevier.com/locate/apsusc

Magnetic studies on ZnTe:Cr film grown on glass substrate by thermal evaporation method

D. Soundararajan [a], D. Mangalaraj [b,*], D. Nataraj [a], L. Dorosinskii [c], J. Santoyo-Salazar [d,e], H.C. Jeon [f], T.W. Kang [f]

[a] Thin Films and Nonmaterials Lab, Department of Physics, Bharathiar University, Coimbatore 641046, India
[b] Department of Nanoscience and Technology, Bharathiar University, Coimbatore 641046, India
[c] National Institute of Metrology (TUBITAK-UME), P.K. 54, 41470, Gebze-Kocaeli, Turkey
[d] Universidad Nacional Autonoma de Mexico, Instituto de Investigaciones en Materiales, Mexico, D.F. AP 70-360, 04510, Mexico
[e] Institut de Physique et Chimie des Matériaux de Strasbourg, UMR CNRS-ULP-ECPM 7504, 23, rue du Loess, BP 43, 67034 Strasbourg cedex, France
[f] Department of Physics, Dongguk University, Seoul 100-715, Republic of Korea

ARTICLE INFO

Article history:
Received 30 September 2008
Received in revised form 4 April 2009
Accepted 6 April 2009
Available online 11 April 2009

Keywords:
Dilute magnetic semiconductors
ZnTe:Cr film
M–H curve
Magnetic domains

ABSTRACT

ZnTe and ZnTe:Cr films were prepared on glass substrate by using thermal evaporation method. X-ray diffraction analysis revealed the presence of ZnCrTe phase. X-ray photoelectron spectroscopy was used to estimate the composition of as-prepared films. The valence state of Cr in ZnTe:Cr film is determined to be +2 by using electron spin resonance spectroscopy. Magnetic moment data as a function of magnetic field was recorded by using superconducting quantum interference device magnetometry at 300 K. The result showed a clear hysteresis loop with coercive field of 48 Oe. Magnetic domains were observed by using magnetic force microscopy and the average value of domain size was 3.7 nm.

1. Introduction

Diluted magnetic semiconductors (DMSs) are the most promising materials for the emerging field of semiconductor spintronics [1,2]. DMSs are compounds based on typical semiconductors (like CdTe or InAs), for which a fraction of nonmagnetic cations has been replaced by magnetic ions (typically transition metal ions like Mn, Fe or rare earth metal ions) [3]. The most relevant feature of DMS, which attracted considerable interest is, the coexistence and interaction with delocalized conduction (s-type) and valence (p-type) band electrons and localized (d- or f-type) electrons of magnetic ions.

So far various kinds of DMS systems were investigated to examine the possibility of practical spintronic applications [4,5]. The main advantage of DMS over ferromagnetic metal (FM) in a metallic spintronic device is the effective spin injection due to smaller lattice mismatch between a DMS and its semiconductor (SC) heterojunction partner and which is unlike the case of spin injection from a FM layer into SC. However, the advantage of DMSs cannot be utilized because their curie temperature is lower than room temperature. A lot of work has been done on the synthesis of novel DMS with room temperature ferromagnetism, based on III–V and II–VI compound semiconductors. Studies on transition metal doped II–VI compound semiconductors is getting attraction, because transition metals have high solubility in this compound semiconductors than in III–V based compound semiconductors [6]. A lot of fundamental studies have been carried out on transition metal doped II–VI semiconductors such as CdTe [7,8] and ZnTe [9,10]. However, only a little application has been realized and this was because of spin glass or antiferromagnetism in these compound semiconductors [11]. Recently, it has been reported that highly 'p' doped ZnTe:Mn films, can show ferromagnetism at 3 K [12] and this was due to the mediation of ferromagnetic ordering between magnetic impurity ions by the added hole carriers [13]. In contrast, when transition metal impurity such as chromium is doped into ZnTe, then the net ferromagnetic exchange interaction has been predicted even without p- or n-type doping [14]. The reason is that Cr dopant created a hole carrier and as well acted as a source of magnetic impurity in ZnTe semiconductor [15]. A detailed theoretical and experimental research works have been done on Cr doped ZnTe thin film [16–22]. Previous results, based on the first principle calculations, has shown that the origin of the ferromagnetism in (Zn,Cr)Te is due to sp–d exchange interaction between sp carriers

* Corresponding author. Tel.: +91 0422 2425458; fax: +91 0422 2422387.
E-mail addresses: devsoundarrajan@yahoo.com (D. Soundararajan), dmraj800@yahoo.com (D. Mangalaraj).

0169-4332/$ – see front matter © 2009 Elsevier B.V. All rights reserved.
doi:10.1016/j.apsusc.2009.04.012

and d-localized electrons [16,17]. Saito et al. have reported that $Zn_{1-x}Cr_xTe$ sample with $x = 0.2$, can exhibits ferromagnetism at room temperature [18–20]. Further, Xie and Liu have studied the half metallic ferromagnetism and stability of zinc blend phase of transition metal doped II–VI compound semiconductors by using density-functional calculation and found that the zincblende Cr doped ZnTe semiconductor and CrTe thin films are excellent half-metallic ferromagnets with wide half-metallic gaps. This half metallic manner leads to ferromagnetic behavior with high Curie temperature [21,22].

In general, ZnTe:Cr thin films were prepared using molecular beam epitaxy (MBE) technique by many researchers [19,20]. In this work, we present a detailed study on the structure and magnetic properties of ZnTe:Cr films prepared on glass substrate by thermal evaporation method. X-ray diffraction study was used to identify the phases in the film. ESR spectroscopy was performed to know the valence state of Cr. Magnetic properties such as magnetic moment measurements as a function of magnetic field, and observation of magnetic domains were done by SQUID magnetometry and MFM, respectively. The obtained results were discussed in this article.

2. Experimental details

2.1. Film preparation

Appropriate weights of high pure Zn, Te and Cr (Alfa Aeser) metals were taken together in two different quartz ampoules for the preparation of $Zn_{1-x}Cr_xTe$ molten alloys with $x = 0.0$, and 0.05. The quartz ampoules were vacuum sealed at a vacuum of 10^{-5} Torr and then the sealed ampoules were kept inside a horizontal tube rotating furnace. In case of pure ZnTe, the vacuum sealed ampoule was maintained at 600 °C for 12 h. In the case of ZnTe:Cr, the ampoule was maintained at 1100 °C for 24 h. In both cases, the temperature of the furnace was slowly increased step by step to the required value and after carrying out the reaction at respective time period, the temperature of the zone was then slowly decreased in steps to room temperature. The molten alloys were taken out and crushed into fine powder by grinding in a mortar. The as obtained ZnTe and ZnTe:Cr were then used for the growth of respective thin films. For this, the as prepared ZnTe and ZnTe:Cr compound powders were taken in tantalum boat source and then tungsten dimple source, respectively, and thermally evaporated onto well cleaned glass substrates under a vacuum of 4×10^{-5} Torr at ambient temperature.

2.2. Characterization techniques

The crystalline structure of the ZnTe and ZnTe:Cr films were analyzed by X-ray diffractometer [Model – Shimadzu (XRD-6000), $\lambda = 1.5406$ Å] operated in the 2θ scan range of 20–80°. In the present study, XPS measurements were carried out using an Escalab 220iXL system (VG Scientific Inc.) with a monochromatic Mg Kα X-ray source (1284.6 eV). The relative atomic percentage of Zn, Te and Cr were obtained by using XPS peak fit software. The optical transmittance spectra of the films were recorded by using a UV–vis–NIR (CARY 2390) spectrophotometer at room temperature. ESR spectroscopy was used to record the first derivative absorption spectra by using an E-112 varian ESR spectrometer at X-band frequency at room temperature. It was measured with a X-band (9.0 GHz) spectrometer in a 100 kHz field modulation. The microwave frequency was kept constant at 9 GHz, while the magnetic field was varied between 0 and 4 mT. Magnetic properties were recorded by using a SQUID magnetometer (Quantum Design MPMS-XL system with 5 T superconducting magnet) at room temperature. Ex-situ topography and magnetic domain measurements were carried out at room temperature by means of scanning probe microscope (SPM) (JEOL JSPM-4210). The particle size and magnetic domains were scanned at room temperature conditions. Topography of films was scanned by AFM in Tapping™ mode and magnetic domains were analyzed by MFM in lift mode with magnetic cantilever tip NSC14/Co–Cr, Mikro-masch, Co. with resonant frequency of 160 kHz. The magnetic domains were observed at a lift interaction height of 25 nm and with an output of 0.025 A/V. The 2D and 3D images, profiles and domains measurements were processed with the win SPM DPS, JEOL Ltd. Software.

3. Results and discussion

3.1. Microstructure

The XRD pattern of ZnTe and ZnTe:Cr films are compared and the results are shown in Fig. 1(a and b). The diffraction pattern of the ZnTe film shows a main peak along (1 1 1) crystallographic direction

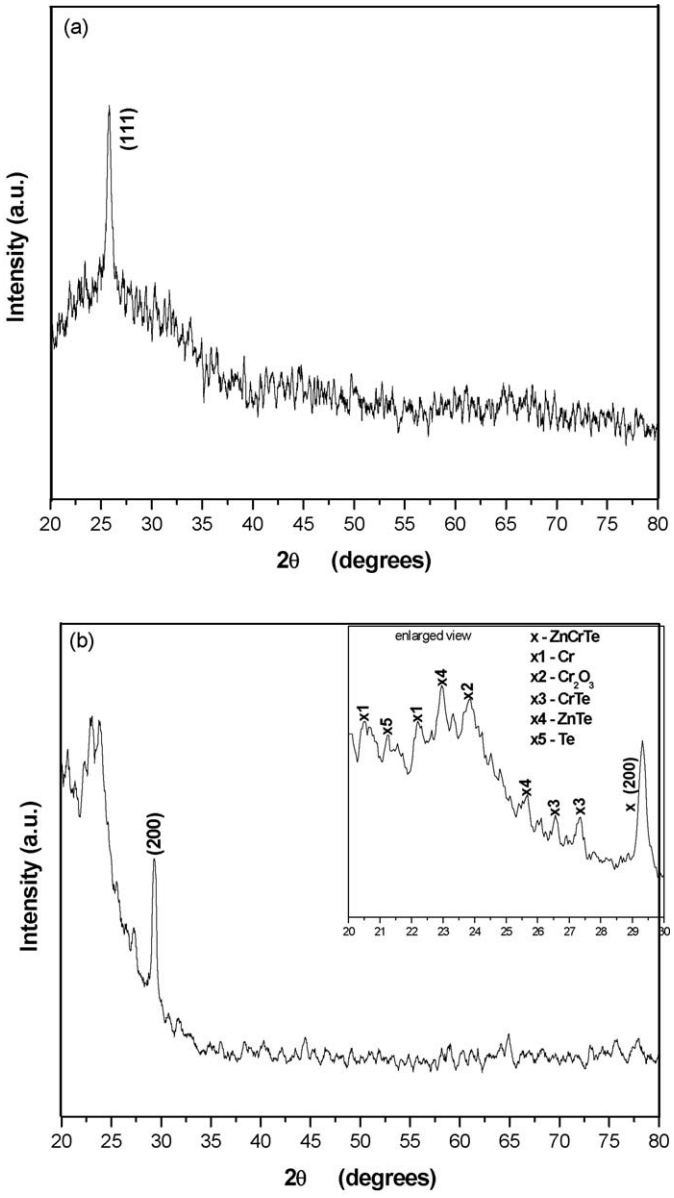

Fig. 1. (a and b) X-ray diffraction patterns of (a) ZnTe and (b) ZnTe:Cr films grown on glass substrate. Inset shows expanded view in the 2θ scan range of 20–30°.

indicating the cubic zinc-blende structure of ZnTe as observed by Akram et al. [23]. In the case of ZnTe:Cr film, poor crystallinity was observed along with a main peak along (2 0 0) crystallographic direction indicating the ZnCrTe cubic zinc blende structure. This peak is similar to a peak observed by Kuroda et al. [24,25] for ZnTe:Cr thin film grown on GaAs (1 0 0) substrate by MBE technique. In addition to the main peak along (2 0 0) crystallographic direction, small peaks were also observed indicating Cr, Cr_2O_3 and CrTe precipitates [26,27]. The calculated lattice parameter values of the ZnTe and ZnTe:Cr films are 5.96 and 6.08 Å, respectively. The change in lattice parameter is an indication that Cr has substitutionally incorporated into the ZnTe lattice.

3.2. XPS spectra

The microscopic surface composition of the prepared $Zn_{1-x}Cr_xTe$ (x = 0, 0.05) films were investigated by high resolution XPS. The results are shown in Figs. 2(a and b) and 3(a–e). The most probable assignments to the origin of components are presented in Tables 1 and 2 [28]. The relative at.% of elements as evaluated from the high resolution spectra using XPS peak fit software are given in Table 3. Fig. 2(a and b) displays the XPS spectra of ZnTe film and it exhibits the characteristic Zn and Te peak positions. There

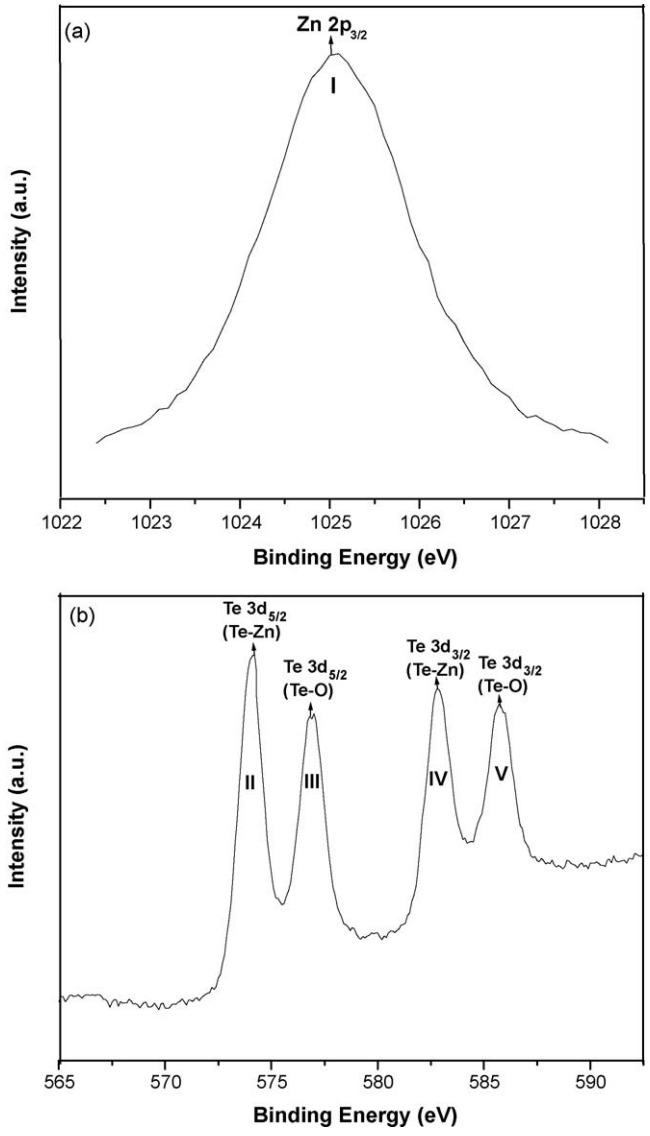

Fig. 2. (a and b) High resolution surface XPS spectra of ZnTe film.

Table 1
Assignments to the component of peaks of the high resolution surface XPS scans of the ZnTe film.

Component	Binding energy (eV)	Assignment
I (Zn $2p_{3/2}$)	1025.08	Zn–Te
II (Te $3d_{5/2}$)	574.2	Te–Zn
IV (Te $3d_{5/2}$)	576.9	Te–O_2
VI (Te $3d_{3/2}$)	582.9	Te–Zn
VIII (Te $3d_{3/2}$)	585.7	Te–O_2

Table 2
Assignments to the component of peaks of the high resolution surface XPS scans of ZnTe:Cr film.

Component	Binding Energy (eV)	Assignment
I (Zn $2p_{3/2}$)	1021.8	Zn–Te
II (Te $3d_{5/2}$)	572.9	Te–Zn
III (Cr $2p_{3/2}$)	574.3	Cr–Te
IV (Te $3d_{5/2}$)	576.5	Te–O_2
V (Cr $2p_{3/2}$)	575.6	Cr_2–O_3
VI (Te $3d_{3/2}$)	583.3	Te–Zn
VII (Cr $2p_{1/2}$)	583.5	Cr–Te
VIII (Te $3d_{3/2}$)	586.5	Te–O_2
IX (Cr $2p_{1/2}$)	586.6	Cr_2–O_3

Table 3
Relative atomic percentage of Zn, Te and Cr elements as evaluated from the high resolution surface XPS spectra of the ZnTe and ZnTe:Cr films.

Samples	Relative at.% of		
	Zn	Te	Cr
ZnTe	52.1	47.17	–
ZnTe:Cr	45.0	50.03	4.97

appeared a single peak for Zn at 1025.08 eV and which corresponds to $2p_{3/2}$ transition. In the case of Te, there appeared two peaks at 574.2 and 582.9 eV and which were corresponds to $3d_{5/2}$ and $3d_{3/2}$ transition, respectively. In addition, in adjacent to these two peaks there appeared another set of peaks at 576.9 and 585.7 eV, which were again corresponds to $3d_{5/2}$ and $3d_{3/2}$ transition but were due to oxide phase of Te (Te-O). A blue shift in the binding energy value of oxide related peaks suggests a fact that Te has donated electrons to oxygen and therefore the binding energy corresponding to $3d_{5/2}$ and $3d_{3/2}$ transitions has been increased. The stoichiometry of the ZnTe films is determined by using the $2p_{3/2}$ peak for Zn and 3d peaks for Te. The calculated value of relative atomic percentage of Zn and Te contents in ZnTe film is 52.1 and 47.17, respectively. This showed that the ZnTe film is slightly rich in Zn. To know the elemental composition, a similar study was also carried out on Cr doped ZnTe film. Fig. 3(a–e) displays the deconvoluted XPS spectra of ZnTe:Cr film. It shows the characteristic Zn, Te and Cr peaks at their corresponding binding energies. Also, the presence of TeO_2 and antiferromangetic Cr_2O_3 components are observed at their corresponding binding energies of 576.5 and 575.6 eV, respectively. The stoichiometry of the ZnTe:Cr film is determined by using the 2p peak for Zn, 3d peaks for Te and 2p peaks for Cr. The estimated value of relative atomic percentage of Zn, Te and Cr contents in ZnTe:Cr film is 45, 50.03 and 4.97, respectively.

3.3. Transmittance spectra and band gap

Transmittance studies were carried out in the wavelength range of 300–1100 nm to investigate the optical absorption properties of the $Zn_{1-x}Cr_xTe$ (x = 0, 0.05) films. The results are plotted in Fig. 4. ZnTe and ZnTe:Cr films show a change in optical transmittance of

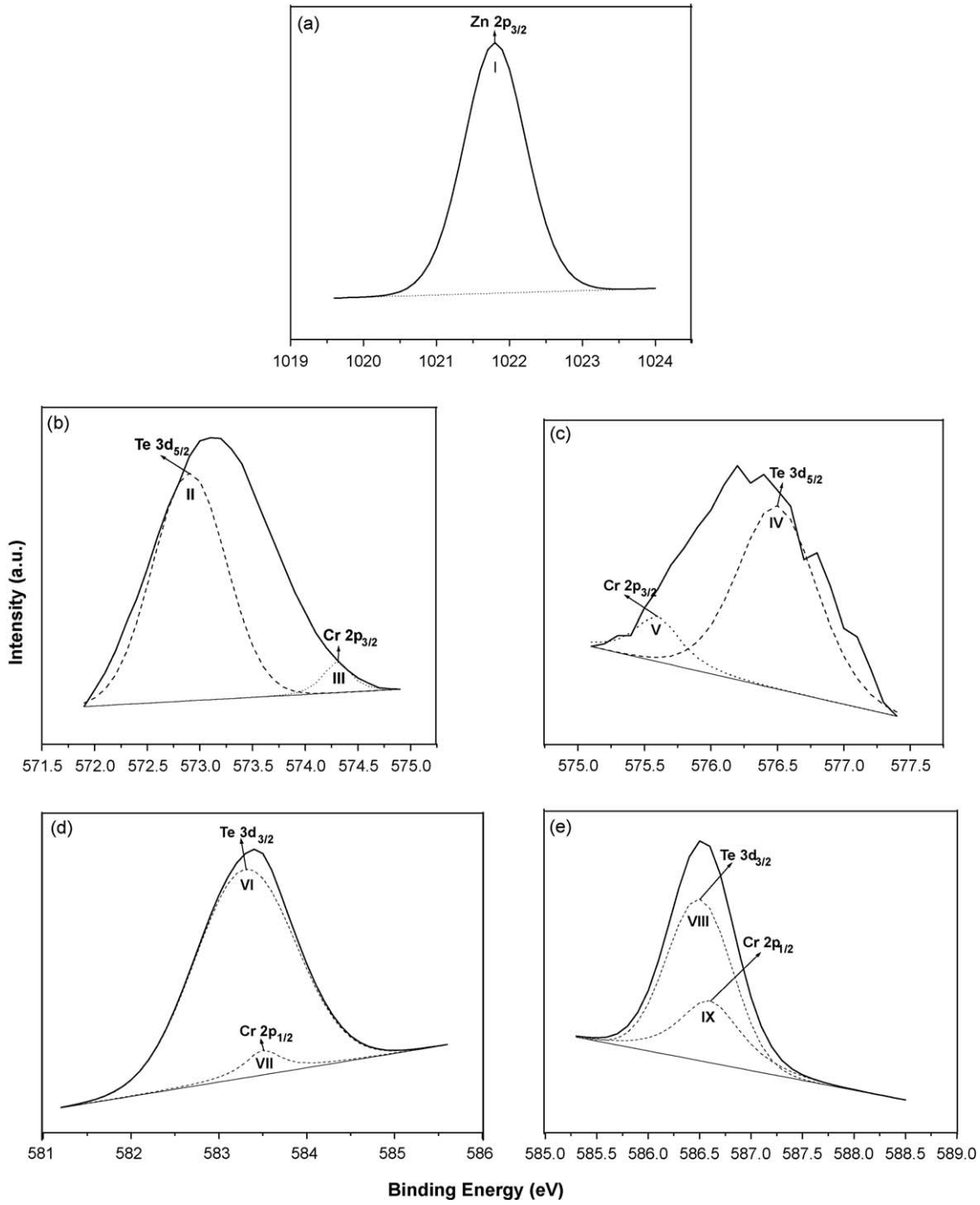

Fig. 3. (a–e) High resolution surface XPS spectra of ZnTe:Cr film.

the films. These changes are attributed to structural, compositional and crystallinity changes in the films when Cr is incorporated into ZnTe lattice. Fundamental absorption edge is found to shift towards lower wavelength region (from 750 to 620 nm) when Cr has been introduced into ZnTe host lattice. The cause of observed blue shift shall be due to the decrease of Zn concentration and increase of Cr concentration in the films. The band gap value has been obtained by the plot between square of absorption coefficient ($(\alpha h\upsilon)^2$) and photon energy ($h\upsilon$) as shown in the inset of Fig. 4. The plot between $(\alpha h\upsilon)^2$ and $h\upsilon$ is found to have straight line over any part of the optical absorption spectrum, thus supporting the interpretation of direct allowed transition [29]. Extrapolation of the linear portion of the curve to $(\alpha h\upsilon)^2 = 0$ gives the optical band gap value for the films. It is observed that the direct band gap energy for undoped ZnTe film is 2.09 eV and it increases to 2.12 eV for Cr doped ZnTe film.

3.4. Magnetic studies

3.4.1. ESR spectra

The advantage of ESR spectroscopy is its great sensitivity to the microscopic environment of the paramagnetic centre and is a tool to know the valence state of Cr in the film so that the origin of magnetic moment from the ZnTe:Cr film can be inferred. The electronic configuration of free Cr atom is $1s^2\ 2s^2\ 2p^6\ 3s^2\ 3p^6\ 3d^5\ 4s^1$. Chromium enters the ZnTe lattice substitutionally for the

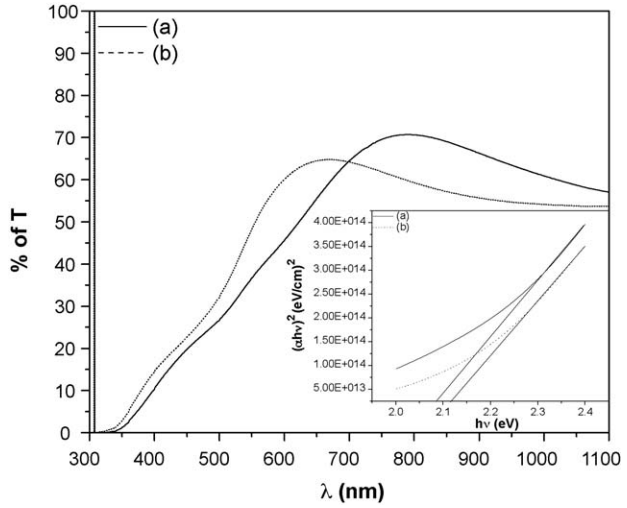

Fig. 4. (a–b) Transmittance spectra of (a) ZnTe and (b) ZnTe:Cr films grown on glass substrate. Inset shows the plot between the square of absorption coefficient and photon energy.

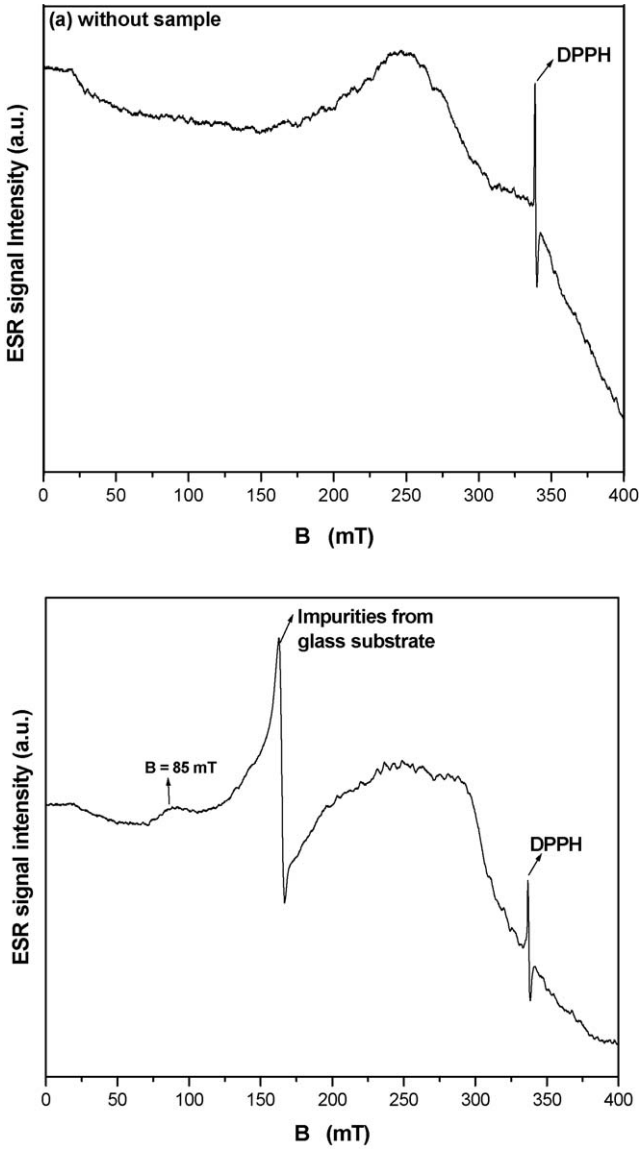

Fig. 5. (a and b) X-band ESR spectra measured (a) without sample and (b) for ZnTe:Cr film on glass at 300 K.

divalent cation and expected in the Cr^{2+} valence state. Fig. 5(a and b) displays the room temperature ESR profiles measured without sample and measured for the ZnTe:Cr film on glass substrate. The spectra of ZnTe:Cr film shows a broad signal which consists of two sharp peaks and a minute unresolved hump at 85 mT. The large sharp signal at B = 163 mT is due to the presence of impurities in the glass substrate [30]. The second small sharp signal at B = 335.3 mT is due to DPPH (2,2-diphenyl-1-picrylhydrazyl) free radical and similar peak is also observed for the ESR spectra without sample. Upon comparing the two ESR spectra, it was found that there is a unresolved minute peak at B = 85 mT for the film and it must be due to the Cr doping effect. The ESR spectrum of the I = 0 chromium isotopes can be analyzed from the following axial spin Hamiltonian

$$H = g_{||}\beta H_{||} + g_{\perp}\beta H_{\perp}$$

The calculated value of $g_{||}$ = 7.90 in the Zeeman interaction term is found at B = 85 mT, which is close to the value 7.92 for Cr^{2+} ion in ZnTe crystal as reported elsewhere [31]. As the calculated $g_{||}$ is similar to earlier reported value, it is assigned to isolated Cr^{2+} ions substitutionally incorporated in the zinc lattice site with the valence state of +2.

3.4.2. M–H curve

Magnetic moment versus magnetic field (M–H) data was obtained at room temperature on ZnTe:Cr film and the result is displayed in Fig. 6. Magnetic moment data are recorded by varying the external magnetic field from 0 to 7000 Oe. The obtained values of coercive field and remanence magnetic moment are 48 Oe and 4.3×10^{-6} emu, respectively. The observed hysteresis loop at room temperature shall originate from the presence of ZnCrTe zinc-blende phase and CrTe related precipitates that are identified from XRD. The X-ray diffraction pattern of Cr doped ZnTe film shows poor crystalline nature with a peak due to ZnCrTe zinc blend phase at 29.5° along (2 0 0) crystallographic direction. The expanded view of diffraction pattern clearly shows the presence of ZnCrTe phase and minute Cr related precipitates such as Cr, Cr_2O_3 and CrTe. The Cr_2O_3 phase is antiferromagnetic stable state of chromium oxide at ambient conditions. However, its metastable phase is chromium dioxide (CrO_2) which is a half metallic ferromagnetic and it becomes Cr_2O_3 at ambient conditions [32].

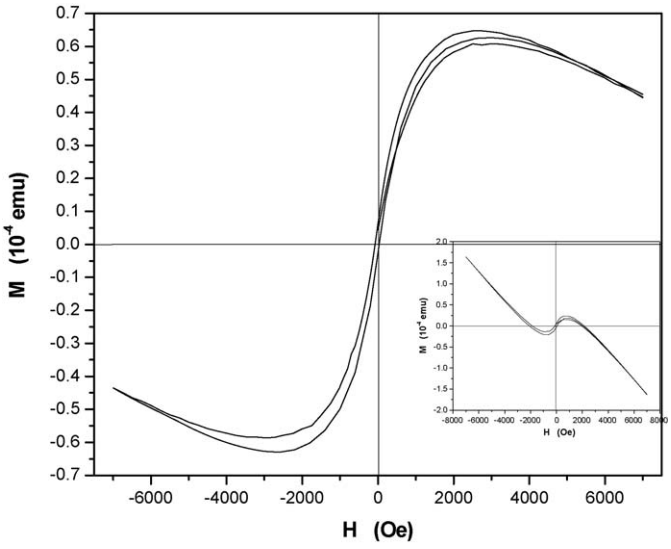

Fig. 6. Magnetic moment versus magnetic field plot of ZnTe:Cr film grown on glass substrate recorded at 300 K. Diamagnetic contribution from the substrate is subtracted. The diamagnetic contribution from ZnTe host lattice was observed in the higher field region. Inset shows the as-obtained M–H curve.

Hence the observed ferromagnetic behavior is expected from ZnCrTe zincblende phase and from CrTe related precipitates. It was already reported that the cubic zincblende crystal structure of ZnCrTe and CrTe are half metallic ferromagnetic with Curie temperature above room temperature and it does a key role in the ferromagnetic behavior of ZnTe:Cr films [33,34]. It is therefore concluded that the presence of zincblende ZnCrTe phase along with minute CrTe related precipitates shall contribute for the observed ferromagnetic behavior at 300 K.

3.4.3. Ferromagnetic domains

In addition to the bulk sensitive *M* versus *H* measurement, surface sensitive magnetic domains was observed by magnetic force microscopy (MFM) on ZnTe:Cr film at room temperature. MFM is becoming one of the most useful techniques for imaging magnetic domains [35]. Prior to MFM analysis, the film was exposed to argon gas blow and consequently the topographic scanning was made by AFM in tapping mode. MFM mode allowed defining the interaction between magnetic domains on the surface of film and the tip. Thus, the topography and magnetic domains were scanned in the same area of 500 nm × 500 nm as shown in Fig. 7(a and b). AFM analysis showed the average particle size as 45 nm. Whereas, MFM images showed small islands as stripe blocks and which were due to magnetic interactions. The stripes inside of islands contain magnetic domains which have different

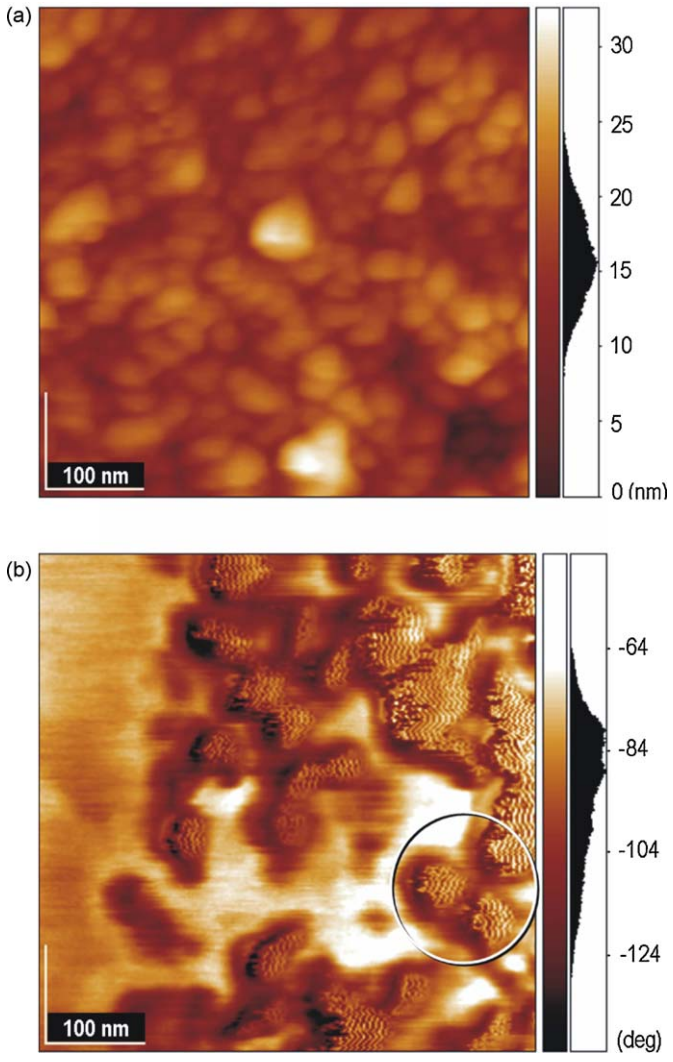

Fig. 7. (a and b) 2D view of (a) AFM and (b) MFM images on ZnTe:Cr film grown on glass substrate recorded in the same region of area 500 nm × 500 nm.

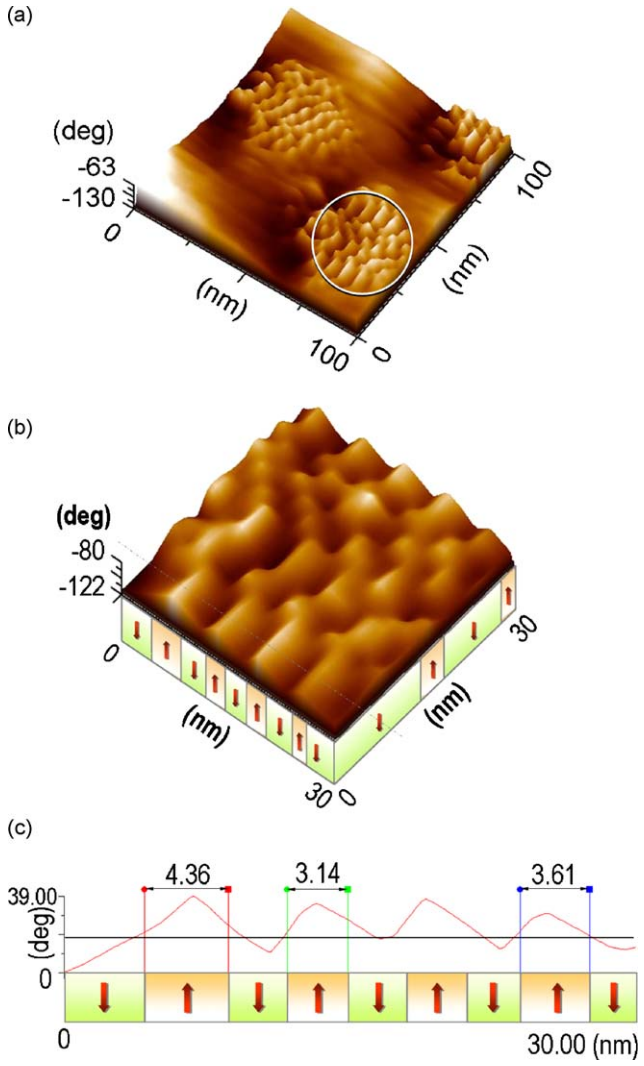

Fig. 8. (a–c) Ferromagnetic multi domains of ZnTe:Cr film grown on glass substrate. (a) 3D view of domains in the surface area of 100 nm × 100 nm (b) selected area 30 nm × 30 nm. (c) Magnetic domains profile in cross section of the image of (b). The magnetic domains measurements correspond to 3.7 nm in average.

positions due to the random distribution of magnetic moments, shape and distribution. The marked region indicated in Fig. 7b was taken in order to analyze the magnetic domains in the island (30 nm × 30 nm) and the zoomed images are shown in Fig. 8(a and b). The shift interaction indicated attractive and repulsive forces between the surface and the tip. Attractive forces were observed as bright block (↑) while, repulsive forces as dark blocks (↓). Fig. 8c shows profile of magnetic domains and which correspond the cross section of the image of Fig. 8b. From this profile pattern, the obtained value of average domains size was 3.7 nm. Though the average grain size value obtained from XRD and AFM analysis are about 45 nm, the average domain size observed by MFM in the marked region is around 3.7 nm. It means that the particles are not single domains, but has several domains of size 3.7 nm. The observed nanometric domain pattern indicates magnetization on the surface of the film. Since a poor crystallinity was observed from XRD, it is believed that the prepared film is not homogeneous and contains nanometric precipitates of CrTe in addition to ZnCrTe zinc-blende phase. These nanometric ferromagnetic phases also play a crucial role in the observed magnetic domains. It is further vital to prepare secondary phase free ZnCrTe films on glass substrate using ZnTe as buffer layer by thermal evaporation

method and subsequently to investigate its structure and magnetic properties.

4. Conclusion

ZnTe and Chromium doped ZnTe films were prepared by thermal evaporation method onto glass substrates and its structure, composition, optical and magnetic properties were studied. Structural investigation by XRD has shown that the formation of ZnCrTe phase, including a minute CrTe, Cr_2O_3 phases. Room temperature magnetic measurements have shown ferromagnetic property in chromium doped ZnTe film and the possible origin of ferromagnetism was from ZnCrTe and a minute CrTe phases, because of their high Curie temperature above room temperature. MFM measurements have shown surface magnetic domains with an average size of 3.7 nm. Since the as obtained magnetic domains size was lower than the particle size calculated, it was also concluded that the particles were not single domains, but consisted of several domains. Thus our preliminary study on thermal evaporated ZnTe:Cr film/glass substrate have shown that ZnTe:Cr can be prepared with room temperature ferromagnetic property. Further investigations are under research, which aims to remove the impurity phases by means of using ZnTe as buffer layer for the growth of ZnTe:Cr films on glass substrate.

Acknowledgement

The authors would like to thank Dr. C. Flores-Morales from Instituto de Investigaciones en Materiales, IIM-UNAM for his technical support in doing AFM/MFM characterization.

References

[1] H. Ohno, A. Shen, F. Matsukura, A. Oiwa, A. Endo, S. Katsumoto, Y. Iye, Appl. Phys. Lett. 69 (1996) 363.
[2] H. Munekata, H. Ohno, R.R. Ruf, R.J. Gambino, L.L. Chang, J. Cryst. Growth 111 (1991) 1011.
[3] L.M. Sandrastskii, P. Bruno, J. Phys. Condens. Matter 15 (2003) L585–L590.
[4] H. Ohno, H. Munekata, T. Penney, S. Von Molna, L.L. Chang, Phys. Rev. Lett. 68 (1992) 664.
[5] I.T. Yoon, T.W. Kang, K.H. Kim, D.J. Kim, Solid State Commun. 130 (2004) 627–630.
[6] I.A. Buyanova, G.Yu. Rudko, W.M. Chen, A.A. Toropov, S.V. Sorokin, S.V. Ivanov, P.S. kop'ev, Appl. Phys. Lett. 82 (2003) 1700.
[7] A. Zozime, M. Seibt, J. Ertel, A. Tromson-Carli, R. Druilhe, C. Grattepain, R. Triboulet, J. Cryst. Growth 249 (2003) 15–22.
[8] S. Mackowski, et al. Appl. Phys. Lett. 83 (2003) 3575.
[9] T. Gurung, S. Mackowski, H.E. Jackson, L.M. Smith, J. Kossut, G. Karczewski, J. Appl. Phys. 96 (2004) 7407.
[10] S. Mackowski, T. Gurung, T.A. Nguyen, H.E. Jackson, L.M. Smith, G. Karczewski, Appl. Phys. Lett. 84 (2004) 3337.
[11] M. Imamura, A. Okada, T. Yamaguchi, J. Appl. Phys. 99 (2006) 08M706.
[12] K. Sato, H. Katayama-Yoshida, Semicond. Sci. Technol. 17 (2002) 367.
[13] K. Ando, H. Saito, V. Zayets, M.C. Debnath, J. Phys. Condens. Matter 15 (2003) R1583.
[14] K. Ando, H. Saito, Z. Jin, T. Fukumura, M. Kawasaki, Y. Matsumoto, H. Komuma, J. Appl. Phys. (NY) 78 (2001) 2700.
[15] X.G. Guo, J.C. Cao, X.S. Chen, W. Lu, Solid State Commun. 138 (2006) 275.
[16] H. Saito, V. Zayets, S. Yamataga, K. Ando, J. Appl. Phys. 93 (2003) 6796.
[17] Q. Wang, Q. Sun, P. Jena, J. Appl. Phys. 97 (2005) 043904.
[18] T. Fukushima, K. Sato, H. Katayama-Yoshida, P.H. Dedirichs, Jpn. J. Appl. Phys. 43 (2004) L1416.
[19] H. Saito, V. Zayets, S. Yamagata, K. Ando, Phys. Rev. B 66 (2002) 081201.
[20] H. Saito, V. Zayets, S. Yamagata, K. Ando, Phys. Rev. Lett. 90 (2003) 207202.
[21] Wen-Hui Xie, Bang-Gui Liu, J. Appl. Phys. 96 (2004) 3559.
[22] Wen-Hui Xie, Ya-Qiong Xu, Bang-Gui Liu, Phys. Rev. Lett. 91 (2003) 037204.
[23] K.S. Akram, Z. Ali, A. Maqsood, Appl. Surf. Sci. 143 (1999) 39.
[24] N. Ozaki, N. Nishzawa, S. Marcet, S. Kuroda, O. Eryu, K. Takita, Phys. Rev. Lett. 97 (2006) 037201.
[25] S. Kuroda, N. Ozaki, N. Nishizawa, T. Kumekawa, S. Marcet, K. Takita, Sci. Technol. Adv. Mater. 6 (2005) 558.
[26] JCPDS, X-ray powder diffraction file, Joint Committee for Powder Diffraction Standards.
[27] H. Ye, Q. Zhang, S. Saito, B. Jeyadevan, K. Tohji, M. Tsunoda, J. Appl. Phys. 93 (2003) 6856.
[28] C.D. Wagner, W.M. Riggs, L.E. Davis, J.F. Moulder, C.E. Muielenberg, Handbook of X-ray Photoelectron Spectroscopy, Physical Electronics Industries, Eden Prairie, MN, 1976.
[29] K. Prabakar, Sa.K. Narayandass, D. Mangalaraj, J. Alloys Compd 364 (2004) 23–28.
[30] M. Diaconu, H. Schmidt, A. Poppl, R. Bottcher, J. Hoentsch, A. Rahm, H. Hochmuth, M. Lorenz, M. Grundmann, Superlatices Microstruct. 38 (2005) 413.
[31] J.T. Vallin, G.A. Slack, S. Roberts, A.E. Hughes, J. Phys. Rev. B 2 (1970) 4313.
[32] D. Stanoi, et al. J. Mater. Sci. Eng. B 118 (2005) 74–78.
[33] W.H. Xie, B.G. Liu, J. Appl. Phys. 96 (2004) 3559.
[34] W.H. Xie, Y.Q. Xu, B.G. Liu, Phys. Rev. Lett. 91 (2003) 037204.
[35] M.H. Ham, S. Yoon, Y. Park, J.M. Myoung, Appl. Surf. Sci. 252 (2006) 6289–6293.